

High-field optically detected nuclear magnetic resonance in GaAs

M. Poggio and D. D. Awschalom
Center for Spintronics and Quantum Computation,
University of California, Santa Barbara, CA 93106
 (Dated: September 5, 2018)

A method for high-field optically detected nuclear magnetic resonance (ODNMR) is developed sensitive to 10^8 nuclei. Nuclear spin transitions are induced using a radio frequency coil and detected through Faraday rotation spectroscopy. Unlike conventional ODNMR, which is limited to low fields and relies on the measurement of time-averaged luminescence polarization, this technique monitors nuclear polarization through time-resolved measurements of electron spin dynamics. Measurements in a (110) GaAs quantum well reveal ^{69}Ga , ^{71}Ga , and ^{75}As resonances and their quadrupolar splittings while resolving changes in nuclear polarization of 0.02%.

PACS numbers: 76.70.Hb, 85.35.Be, 78.47.+p, 76.60.Jx

The small number of nuclear spins in quantum wells (QWs) and quantum dots makes conventional nuclear magnetic resonance (NMR) experiments difficult in these semiconductor nanostructures. Optical pumping¹ strongly enhances nuclear spin polarization and can increase the detection sensitivity of typical radio frequency (RF) probes from a minimum of 10^{17} nuclear spins to 10^{12} . As a result, RF detection of optically pumped GaAs multiple QWs has been achieved². Detection of NMR has also been demonstrated through optical measurements of recombination polarization, either by exciting NMR transitions with a conventional coil^{3,4}, or by purely optical means^{5,6,7,8}. In the latter case, an optical field is modulated at the nuclear Larmor frequency resulting in an oscillating electron magnetization. This magnetization interacts with nuclear spins through the contact hyperfine coupling and induces NMR transitions in lieu of an external RF field. While optically detected NMR (ODNMR) provides the high sensitivity typical of optical techniques, it has several limitations. For electron g-factors and spin lifetimes typical of GaAs structures, ODNMR is only possible at low magnetic fields (< 1 T). In addition, the reliance on radiative recombination for detection makes ODNMR disproportionately sensitive to nuclei located near shallow donors and impurities⁹.

Another type of ODNMR is possible using time-resolved Faraday rotation (FR)¹⁰ to probe nuclear spin polarization. In this detection scheme, FR measures the spin precession frequency of electrons in the conduction band. Nuclear spins act on electron spins through the contact hyperfine interaction altering this frequency and allowing for the precise measurement of nuclear polarization. All-optical versions of this method have been demonstrated in bulk GaAs and in a GaAs QW^{11,12,13}. These measurements can be made at high applied magnetic fields and, unlike measurements of time- and polarization-resolved photoluminescence, they are not limited by the charge recombination time.

Here we present an extension of this technique utilizing an RF coil for the excitation of NMR transitions. The use of an external RF field allows for the future application of well-developed pulsed NMR techniques for

noise reduction while at the same time exploiting the high sensitivity of FR detection. In addition, the conventional magnetic excitation of nuclear transitions circumvents the complex interactions between electrons and nuclei which take place in optical excitation schemes. Unlike conventional RF magnetic fields, which induce only dipole transitions, modulated optical fields induce both magnetic dipole transitions and electric quadrupole transitions^{8,12,13,14}.

As shown in Fig. 1, a semiconductor sample is cooled to $T = 5$ K in a magneto-optical cryostat with an applied magnetic field \vec{B}_0 along the z-axis and is mounted in the center of a 10 mm \times 5 mm Helmholtz coil wound from 22 AWG magnet wire. RF radiation is coupled to the coil from the top of the cryostat through an impedance-matched semi-rigid coaxial transmission line producing an RF magnetic field \vec{B}_1 along the y-axis. The sample growth direction lies in the xz-plane and can be rotated to adjust the angle α between the growth direction and the laser propagation direction along the x-axis. Unless otherwise specified $\alpha = 10^\circ$.

We measure time resolved FR in a modulation doped 7.5-nm wide (110) GaAs QW with a mobility of 1700 cm²

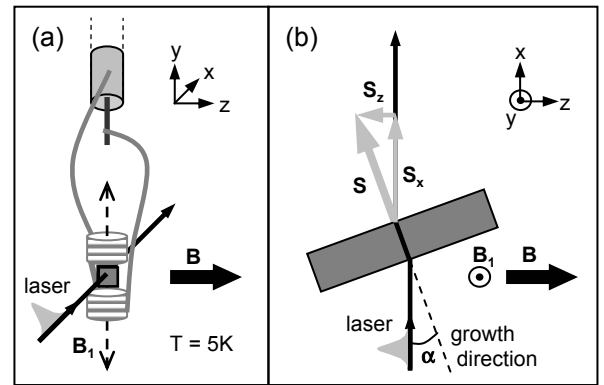


FIG. 1: Schematic of the experimental geometry. (a) Side view of the apparatus within a magneto-optical cryostat. (b) Top view of the sample at the center of the Helmholtz coil.

$V^{-1} \text{ s}^{-1}$ and an electron density of $9 \times 10^{10} \text{ cm}^{-2}$ at $T = 300 \text{ S K}$. Confinement along the (110) crystal direction suppresses D'yakonov-Perel spin scattering resulting in spin lifetimes longer than 1 ns from $T = 5 \text{ K}$ to room temperature¹⁶. A 250-fs 76-MHz Ti:Sapphire laser tuned near the exciton absorption energy (1.572 eV) produces pulses which are split into pump and probe with a full width at half maximum (FWHM) of 8 meV and an average power of 2.0 mW and 100 μW respectively. The linearly (circularly) polarized probe (pump) is modulated by an optical chopper at $f_1 = 940 \text{ Hz}$ ($f_2 = 3.12 \text{ kHz}$). Both beams are focused on the sample surface to an overlapping spot 50 μm in diameter with the pump beam injecting polarized electron spins along the sample growth direction as shown in Fig. 1b. The pinning of the of the initial electron spin polarization \vec{S} along the growth direction relies on the fact that pump pulses couple predominantly to heavy hole states, which are split off from light holes states in a QW^{13,15}. Small rotations in the linear polarization of the transmitted probe are measured and are proportional to the component of electron spin polarization in the conduction band along the growth direction. Variation of the pump-probe time delay Δt reveals the time evolution of this spin polarization. In the absence of nuclear polarization, electron spins precess about an axis and at a frequency defined by the Larmor precession vector $\vec{\nu}_L = \hat{g}\vec{B}_0\mu_B/h$, where \hat{g} is the Landé g-factor expressed as a tensor, μ_B is the Bohr magneton, and h is Planck's constant. GaAs QWs grown in the (110) direction exhibit strong anisotropy in \hat{g} resulting in both the dependence of ν_L on the orientation of \vec{B}_0 with respect to the sample's crystal axes and in a difference between the precession axis $\vec{\nu}_L$ and the direction of \vec{B}_0 ¹³.

At $T = 5 \text{ K}$, spin-polarized photo-excited electrons generate nuclear spin polarization within the QW through dynamic nuclear polarization (DNP)¹. DNP acts through the contact hyperfine interaction, written as $A_H \vec{I} \cdot \vec{S} = \frac{1}{2} A_H (I^+ S^- + I^- S^+) + A_H I_z S_z$, where A_H is the hyperfine constant and \vec{I} is the nuclear spin. This “flip-flop” process results in an average nuclear spin $\langle \vec{I} \rangle$ along \vec{B}_0 and is driven by the component of electron spin S_z in that direction. The sign and magnitude of $\langle \vec{I} \rangle$ depends on the angle α .

The presence of a non-zero $\langle \vec{I} \rangle$ in turn acts on the electron spin dynamics through the addition of a term to the precession vector $\vec{\nu}_L = \hat{g}\vec{B}_0\mu_B/h + A_H \langle \vec{I} \rangle / h$. The measurement of ν_L and the knowledge of \hat{g} and \vec{B}_0 yield the nuclear polarization frequency $\nu_n = A_H \langle I \rangle / h$, which has been calculated to be 32.6 GHz for 100% nuclear polarization in GaAs⁴. Changes in the average nuclear polarization $\langle I \rangle / I$ within the QW can be measured directly as changes in the precession frequency $\Delta \nu_L$.

FR is plotted in Fig. 2a as a function of Δt at $B_0 = 5.3019 \text{ T}$ with the coil driven continuously at a frequency f_c set to the ^{69}Ga resonance at 50.0000 MHz and at two frequencies slightly detuned from resonance.

The inset clarifies the reduction of ν_L for the resonant scan in which nuclear spin transitions induced by B_1 decrease $\langle I \rangle$. Scans with an off-resonant f_c , show the same $\langle I \rangle$ established by DNP without any applied B_1 . Fig. 2b shows FR data taken under the same conditions as in Fig. 2 while sweeping f_c across the ^{69}Ga resonance at a fixed $\Delta t = 1932 \text{ ps}$. Here, the resonant depolarization of $\langle I \rangle$ and the change in ν_L appear as a peak in the FR signal. The asymmetry of the resonance reflects the fast rate of the frequency sweep with respect to the time required to polarize the nuclei $T_{DNP} \sim 90 \text{ s}$. In order to investigate the true form of the peak, f_c is swept across the full

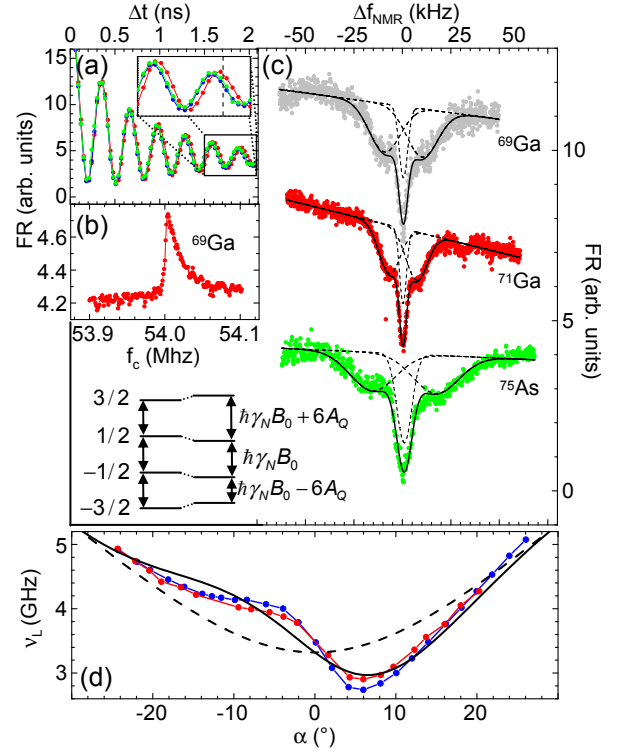


FIG. 2: (Color) NMR detected by time-resolved FR. (a) FR data taken at $B_0 = 5.3019 \text{ T}$ with B_1 driven at 54.0000 MHz, 50.0400 MHz, and 53.9800 MHz for the red, blue, and green points respectively. Lines connect the data to guide the eye. (b) FR shown as a function of f_c for fixed $\Delta t = 1932 \text{ ps}$ as indicated by the dashed line in the inset to (a). (c) FR plotted as a function of detuning Δf_{NMR} from the ^{69}Ga resonance of 52.9539 MHz at $B_0 = 5.2 \text{ T}$, from the ^{71}Ga resonance of 67.2898 MHz at $B_0 = 5.2 \text{ T}$, and from the ^{75}As resonance of 54.4992 MHz at $B_0 = 7.5 \text{ T}$ for the gray, red, and green points respectively. Solid black lines are fits to the data while dashed lines show the three peaks included in those fits. A schematic diagram of the relevant level structure is included in the lower left. (d) ν_L shown as a function of α at $B_0 = 5.5 \text{ T}$ for no RF voltage applied to the coil and for -15 dBm applied at the ^{69}Ga resonance at 56.0070 MHz for the blue and red points respectively. The solid black line is a fit to the angular dependence of ν_L in the presence of a non-zero $\langle I \rangle$. The dashed black line shows the same dependence with $\langle I \rangle = 0$.

nuclear resonance in a time $T_{sweep} \gg T_{DNP}$. This condition is satisfied for the data shown in Fig. 2c where the resonances due to the three isotopes present in the QW, ^{69}Ga , ^{71}Ga , and ^{75}As , appear at the expected frequencies. In addition we observe satellite peaks for each resonance due to the quadrupolar splitting $6A_Q$. By fitting each resonance to a Gaussian peak and two symmetric satellites, the splittings are measured to be 9.7 kHz, 7.0 kHz, and 16.3 kHz for the ^{69}Ga , ^{71}Ga , and ^{75}As isotopes. These values are similar to previously reported measurements and indicate the presence of a small amount of strain on the crystal likely due to the wax used in mounting the sample¹⁷. The line-width (FWHM) of the main resonance is 2.6 kHz, 2.1 kHz, and 4.6 kHz for the ^{69}Ga , ^{71}Ga , and ^{75}As isotopes respectively. The line-widths of the satellite peaks are broader at 9.4 kHz, 6.5 kHz, and 13.8 kHz probably because of inhomogeneous strain in the sample. As noted elsewhere¹⁷, methods such as ours for accurately measuring A_Q are useful in the determination of built-in strain in semiconductor heterostructures.

The dependence of ν_L on α is shown in Fig. 2d in the case of no RF voltage applied to the transmission line and in the case of -15 dBm applied at the ^{69}Ga resonance $f_c = 5.0070$ MHz for $B_0 = 5.5$ T. The solid black line is an angle dependence calculated according to Salis et al. taking into account an anisotropic \hat{g} and a 9% nuclear spin polarization. The calculation reproduces the qualitative features of the data and confirms the dependence of DNP on α . This analysis also leads to the conclusion that the curve taken with the coil resonantly depolarizing the ^{69}Ga nuclei has a nuclear polarization of 6–7%. Since the natural abundance of ^{69}Ga is 0.3, we can say that the RF coil is close to achieving full depolarization of the resonant isotope within the QW.

A conventional ODNMR measurement was made in order to compare its sensitivity to the FR-based scheme. In this case, a sample of bulk semi-insulating (100) GaAs is used instead of a QW due to the lower expected sensitivity of the photoluminescence (PL) technique. 5 mW of circularly polarized light from a CW Ti:Sapphire laser tuned to 1.570 eV is focused to a 100 μm diameter spot on the sample surface. For this experiment, the sample geometry is the same as shown in Fig. 1 with $\alpha = 20^\circ$. Instead of collecting a transmitted probe beam, here the polarization of the PL ρ emitted by the sample along the x-axis is measured using a 40 kHz photo-elastic modulator, followed by a linear polarizer, and a spectrometer with a photo-multiplier tube. Emission from the excitonic peak at 1.514 eV is collected at 5 K as a function of B_0 .

Fig. 3a shows ρ as a function of B_0 with B_1 driven at f_c . The Hanle effect data shown here is typical of GaAs in the presence of DNP¹⁸ and clearly illustrates the resonant depolarization at the isotopic NMR frequencies. Electron spin precession causes the time-averaged spin vector, and thus ρ , to decrease in an increasing transverse magnetic field. By the same reasoning, ρ is sensitive to the effective transverse magnetic field B_n due to $\langle I \rangle$. The broad peak

seen around 20 mT in Fig. 3 is a result of B_n directly opposing and compensating B_0 . The peaks shown to shift as a function of f_c are due to a decrease in B_n under the resonant depolarization of $\langle I \rangle$. The 10 kHz/mT shift in the resonance for small f_c is close to the gyromagnetic ratio of the three relevant isotopes. As f_c increases, the splitting between resonances increases until at $f_c = 100$ kHz and $f_c = 120$ kHz, the three resonances are clearly distinguishable.

A calculation of the Hanle effect based on typical bulk GaAs parameters and the three NMR resonances is shown in Fig. 3b. There is good qualitative agreement between the model and the data allowing us to estimate $\langle I \rangle / I \sim 0.25\%$ as shown in the dependence predicted by the model in Fig. 3c. The signal-to-noise in the data indicates that we are sensitive to changes down to 0.05%. Since the region from which we are collecting PL contains $\sim 10^{16}$ nuclei, we estimate a sensitivity of 10^{12} nuclear spins for this ODNMR technique. In the FR measurement, which was done in a QW, we probed many fewer nuclei, $\sim 10^{12}$. There we could distinguish nuclear polarizations as small as 0.015% corresponding to a sensitivity of 10^8 nuclear spins.

In conclusion, ODNMR detected by time-resolved FR is an extremely sensitive probe of nuclear polarization capable of resolving small numbers of nuclear spins and distinguishing quadrupolar splittings in the kHz range. It may find use in the determination of built-in strain in GaAs heterostructures and provides an excellent way to

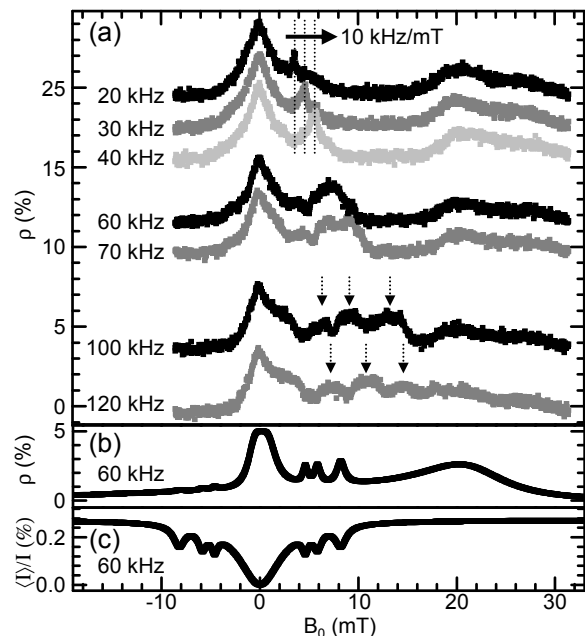


FIG. 3: NMR detected by time-averaged PL polarization. (a) ρ taken as B_0 is swept from -10 mT to 30 mT at 2 mT/min for different values of f_c . (b) A calculation of ρ as a function of B_0 is shown along with the corresponding (c) dependence of $\langle I \rangle / I$ on B_0 . The dip around $B_0 = 0$ T is due to the emergence of nuclear spin-spin coupling at low fields.

perform ODNMR measurements at high magnetic fields, impossible by conventional techniques based on PL polarization.

Acknowledgments

We thank Y. Ohno and H. Ohno for providing the samples, G. M. Steeves for his assistance in running the ex-

periment, S. K. Buratto, and G. Salis for helpful discussions, and we acknowledge support from DARPA, ONR, and NSF.

-
- ¹ G. Lampel, Phys. Rev. Lett. **20**, 491 (1968).
² S. E. Barrett, R. Tycko, L. N. Pfeiffer, and K. W. West, Phys. Rev. Lett. **72**, 1368 (1994).
³ A. I. Ekimov and V. I. Safarov, Zh. Eksp. Teor. Fiz. Pis'ma **15**, 257 (1972) [JETP Lett. **15**, 179 (1972)].
⁴ D. Paget, G. Lampel, B. Sapoval, and V. I. Safarov, Phys. Rev. B **15**, 5780 (1977).
⁵ V. K. Kalevich, V. D. Kul'kov, and V. G. Fleisher, Sov. Phys. Solid State **22**, 703 (1980).
⁶ V. K. Kalevich, V. D. Kul'kov, and V. G. Fleisher, Sov. Phys. Solid State **23**, 892 (1981).
⁷ V. K. Kalevich, Sov. Phys. Solid State **28**, 1947 (1986).
⁸ M. Eickhoff, B. Lenzman, G. Flinn, and D. Suter, Phys. Rev. G **65**, 125301 (2002).
⁹ D. Paget, Phys. Rev. B **25**, 4444 (1982).
¹⁰ S. A. Crooker, D. D. Awschalom, J. J. Baumberg, F. Flack, and N. Samarth, Phys. Rev. B **56**, 7574 (1997).
¹¹ J. M. Kikkawa and D. D. Awschalom, Science **287**, 473 (2000).
¹² G. Salis, D. T. Fuchs, J. M. Kikkawa, D. D. Awschalom, Y. Ohno, and H. Ohno, Phys. Rev. Lett. **86**, 2677 (2001).
¹³ G. Salis, D. D. Awschalom, Y. Ohno, and H. Ohno, Phys. Rev. B **64**, 195304 (2001).
¹⁴ M. Poggio, G. M. Steeves, R. C. Myers, Y. Kato, A. C. Gossard, and D. D. Awschalom, Phys. Rev. Lett. **91**, 207602 (2003).
¹⁵ X. Marie, T. Amand, J. Barrau, P. Renucci, and P. Lejeune, Phys. Rev. B **61**, 11605 (2000).
¹⁶ Y. Ohno, R. Terauchi, T. Adachi, F. Matsukura, and H. Ohno, Phys. Rev. Lett. **83**, 4196 (1999).
¹⁷ D. J. Guerrier and R. T. Harley, Appl. Phys. Lett. **70** 1739 (1997).
¹⁸ *Optical Orientation*, edited by F. Meier and B. P. Zakharchenya (Elsevier, Amsterdam, 1984).